Electron–phonon interaction in atomic-scale conductors: Einstein oscillators versus full phonon modes

2003 J. Phys.: Condens. Matter 15 8781

(http://iopscience.iop.org/0953-8984/15/50/011)

INSTITUTE OF PHYSICS PUBLISHING JOURNAL OF PHYSICS: CONDENSED MATTER

J. Phys.: Condens. Matter **15** (2003) 8781–8795 PII: S0953-8984(03)66835-9

Electron–phonon interaction in atomic-scale conductors: Einstein oscillators versus full phonon modes

M J Montgomery and T N Todorov

School of Mathematics and Physics, Queen's University of Belfast, Belfast BT7 1NN, UK

Received 30 July 2003
Published 3 December 2003
Online at stacks.iop.org/JPhysCM/15/8781

Abstract

Two extreme pictures of electron–phonon interactions in nanoscale conductors are compared: one in which the vibrations are treated as independent Einstein atomic oscillators, and one in which electrons are allowed to couple to the full, extended phonon modes of the conductor. It is shown that, under a broad range of conditions, the full-mode picture and the Einstein picture produce essentially the same net power at any given atom in the nanojunction. The two pictures begin to differ significantly in the limit of low lattice temperature and low applied voltages, where electron–phonon scattering is controlled by the detailed phonon energy spectrum. As an illustration of the behaviour in this limit, we study the competition between trapped vibrational modes and extended modes in shaping the inelastic current–voltage characteristics of one-dimensional atomic wires.

1. Introduction

In recent years there has been a growing recognition of the fact that the passage of electrical current through a nanoscale conductor can have a significant effect on the mechanical properties of the conductor. One such effect is current-induced forces and their influence on the structure and stability of the nanoconductor. In this paper, we are concerned with the other principal current-induced mechanical effect: inelastic electron–phonon scattering in atomic wires and the resultant local power dissipation [1].

Early experimental evidence for local heating in nanowires came from observations of the voltage dependence of two-level conductance fluctuations and hysteresis at conductance steps during the pull-off or compression of an atomic-scale metallic contact [2, 3]. The possibility that even a defect-free, ballistic nanoscale conductor could undergo substantial local heating in the presence of current immediately raises the question of how such local power dissipation might affect the stability of these elemental conductors. There has indeed been growing evidence for current-induced fracture or structural modification of atomic wires and

0953-8984/03/508781+15$30.00

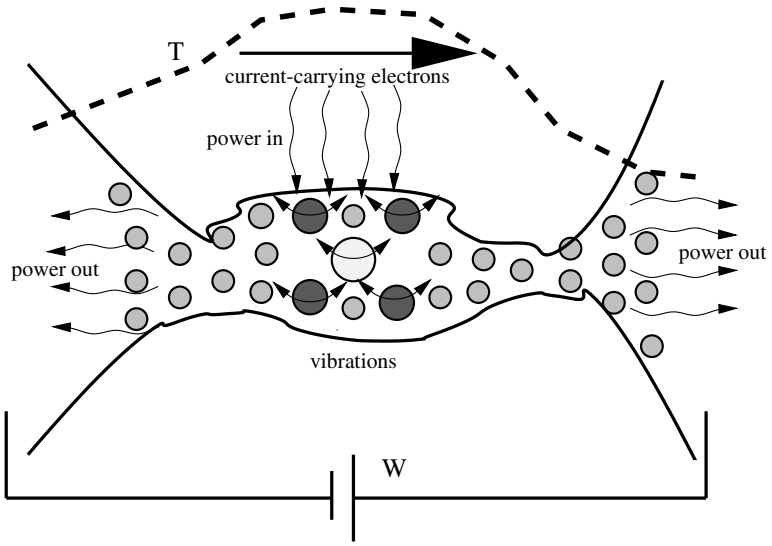

Figure 1. The set-up for the description of electron–phonon interactions and local power dissipation in nanoscale conductors, as considered in the paper.

point-contacts [4–10]. The second principal experimental question to which electron–phonon interactions are relevant is inelastic current–voltage spectroscopy of atomic wires [11, 12] and molecular junctions [13, 14].

Let us now turn to one widely used notional set-up for the description of inelastic electron–phonon scattering and power dissipation in nanojunctions, depicted in figure 1. We picture a general nanoscale junction between two electrodes under an applied bias, W. The bias results in the flow of electrical current. In its simplest form, the argument then runs through two steps. First, the junction is characterized by a set of vibrational modes. Inelastic interactions between the current-carrying electrons and these modes result in net power dissipation into the junction, designated as 'power in' in figure 1. Second, the vibrational modes of the junction are coupled to the adjoining electrodes. This enables heat flow out of the junction, designated as 'power out' in the figure. Balancing power in against power out enables one to obtain an estimate of the steady-state temperature profile, T, in the junction in the presence of current. This approach has been applied to current-induced heating of isolated defects [15–17]. It has also been used to model local heating of current-carrying nanoscale metallic contacts and nanowires [18, 19]. Recently, it has been applied to molecular junctions [20].

Power in, in figure 1, can be calculated by first-order perturbation theory of the interaction between current-carrying electrons and vibrations in the junction. In the past, this calculation has been implemented in two different ways. In simple treatments, the vibrations have been described as independent atomic Einstein oscillators [18, 19]. In more elaborate treatments, the electrons have been coupled to the full phonon modes of the junction [20, 21]. The purpose of this paper is to examine the similarities and differences between these two pictures. We demonstrate that, in the limit $|eW| \gg kT$, $|eW| \gg \hbar\omega$ where ω is a typical vibrational frequency, the two pictures lead to essentially identical values for the net power dissipated by the current at a given atom in the nanojunction. The equivalence of the two pictures is lost away from the above limits. If $|eW|$ is comparable to $\hbar\omega$, then electron–phonon interactions are controlled by the detailed properties of the individual full phonon modes of the junction.

As an illustration, we study the competition between trapped modes and extended modes in shaping the inelastic current–voltage curves of defective low-dimensional atomic wires. We show that, in short wires, bound phonons can dominate the inelastic current–voltage features. As the wire length increases, however, and phonon and electron momentum become better and better quantum numbers, the inelastic current–voltage characteristics become dominated by scattering off extended plane-wave phonons with a wavevector set by the requirement of total momentum conservation.

2. Formalism

2.1. The general set-up

We begin by outlining the perturbative electron–phonon scattering calculation that underlies the calculation of power dissipation, both into full phonon modes and into Einstein oscillators. The formalism follows [19, 21] closely. In those papers, the formalism was developed with explicit reference to a simple tight-binding electronic model. We will, later on, use such simple models to illustrate our analytical derivations by numerical calculations. However, the formalism itself will first be presented in a general way, independent of the underlying electronic model.

To apply perturbation theory to the electron–phonon interaction, we must first define a reference unperturbed state for the electron–phonon system. In this unperturbed state, the electrons and phonons are treated as two independent, decoupled systems. To define the unperturbed state of the electron subsystem, we imagine that all ions are frozen in their equilibrium positions. The electron eigenstates for the electrode–junction–electrode system in figure 1 can, quite generally, be divided into two classes [22]. The states in one class, $\{|\psi_1\rangle\}$ with energies $\{E_1\}$, consist of a right-travelling wave, incident in the left electrode upon the junction, then partially reflected back into the left electrode and partially transmitted into the right electrode, and conversely for the other class, $\{|\psi_2\rangle\}$ with energies $\{E_2\}$. To set up current flow we imagine that the battery in figure 1 populates the states $\{|\psi_1\rangle\}$ and $\{|\psi_2\rangle\}$ with Fermi–Dirac occupation functions $f_1(E)$ and $f_2(E) = f_1(E + eW)$, with electrochemical potentials μ_1 and $\mu_2 = \mu_1 - eW$, respectively. The electronic structure of the current-carrying electrode–junction–electrode system in the absence of electron–phonon interactions is thus described by the density operator

$$\rho(W) = \int f_1(E)D_1(E)\,\mathrm{d}E + \int f_2(E)D_2(E)\,\mathrm{d}E \tag{1}$$

where

$$D_1(E) = \sum_1 |\psi_1\rangle\delta(E - E_1)\langle\psi_1|, \qquad D_2(E) = \sum_2 |\psi_2\rangle\delta(E - E_2)\langle\psi_2| \tag{2}$$

are the partial density of states operators associated with the two classes of electron states. $D_1(E)$ and $D_2(E)$, and the total density of states operator $D(E) = D_1(E) + D_2(E)$, can, ultimately, be expressed in terms of the Green function for the electrode–junction–electrode system [19, 21, 22].

The unperturbed atomic vibrations are described by a phonon Hamiltonian of the form

$$H_z = \sum_{n,\nu} p_{n\nu}^2/2M_n + \sum_{n,\nu,m,\mu} u_{n\nu}K_{n\nu m\mu}u_{m\mu}/2. \tag{3}$$

Here, $u_{n\nu}$ and $p_{n\nu}$ are the displacement and the momentum, respectively, of atom n in direction ν. M_n is the mass of the atom. The real symmetric matrix $\mathbf{K}$ with elements $K_{n\nu m\mu}$ is the

dynamical response matrix, defined as

$$K_{n\nu m\mu} = -\partial F_{n\nu}/\partial u_{m\mu}, \tag{4}$$

where $\mathbf{F_n} = (F_{nx}, F_{ny}, F_{nz})$ is the force on atom n that results from a displacement of atom m by an amount $\mathbf{u_m} = (u_{mx}, u_{my}, u_{mz})$ [21]. In this paper, we ignore any possible effect of the current on $\mathbf{K}$. This assumption may need to be revised in the limit of high voltages, where current-induced corrections to interatomic forces can be significant [23–25].

The electron and phonon subsystems are now coupled by an appropriate interaction term, of the general form [19, 21]

$$V_{\mathrm{ez}} = \sum_{n,\nu} V_{n\nu} u_{n\nu} \tag{5}$$

where $V_{n\nu} = V_{n\nu}^{\dagger}$ is an operator acting on the electron states. Explicit forms for $V_{n\nu}$ will be considered in the numerical calculations later on.

2.2. Power into full phonon modes

Once we have the dynamical response matrix $\mathbf{K}$ for the nanojunction, the phonon modes of the junction may be obtained as follows. If the masses of the junction atoms are not all the same, first it is necessary to make the transformations

$$\tilde{p}_{n\nu} = p_{n\nu}\big/\sqrt{M_n}, \qquad \tilde{u}_{n\nu} = u_{n\nu}\sqrt{M_n} \tag{6}$$

$$\tilde{K}_{n\nu m\mu} = K_{n\nu m\mu}\big/\sqrt{M_n M_m} \tag{7}$$

$$\tilde{V}_{n\nu} = V_{n\nu}\big/\sqrt{M_n} \tag{8}$$

in terms of which equations (3) and (5) become

$$H_{\mathrm{z}} = \sum_{n,\nu} \tilde{p}_{n\nu}^2/2 + \sum_{n,\nu,m,\mu} \tilde{u}_{n\nu}\tilde{K}_{n\nu m\mu}\tilde{u}_{m\mu}/2 \tag{9}$$

$$V_{\mathrm{ez}} = \sum_{n,\nu} \tilde{V}_{n\nu}\tilde{u}_{n\nu}. \tag{10}$$

The phonons are quantized by imposing

$$[\tilde{u}_{m\mu}, \tilde{p}_{n\nu}] = \mathrm{i}\hbar\delta_{mn}\delta_{\mu\nu}. \tag{11}$$

In what follows it will occasionally be convenient to employ a single index, i, instead of the double index $n\nu$ for the atomic degrees of freedom, in such a way that there is a unique value of i for every $n\nu$. Let now $\mathcal{M}_{ji}$ be component i of eigenvector j, normalized to unity, of the matrix $\tilde{\mathbf{K}}$ in equation (7), so that

$$\sum_i \tilde{K}_{li}\mathcal{M}_{ji} = \tilde{K}_j\mathcal{M}_{jl} \tag{12}$$

where $\tilde{K}_j$ is the eigenvalue corresponding to eigenvector j. The matrix $\boldsymbol{\mathcal{M}}$ is unitary. In what follows, index j will always be used to label phonon modes. Index j has the same number of values as the composite index $i \equiv n\nu$, used to label the individual atomic degrees of freedom. Then $\mathcal{M}_{ji}$ gives the normalized amplitude of phonon mode j at atom n, in direction ν. The angular frequency, ω_j, of phonon mode j is given by

$$\omega_j^2 = \tilde{K}_j. \tag{13}$$

We now introduce the phonon creation and annihilation operators

$$A_j^\dagger = \sum_i \left(\sqrt{\omega_j/2\hbar}\mathcal{M}_{ji}\tilde{u}_i - \mathrm{i}\sqrt{1/2\hbar\omega_j}\mathcal{M}_{ji}^*\tilde{p}_i \right) \tag{14}$$

$$A_j = \sum_i \left(\sqrt{\omega_j/2\hbar}\mathcal{M}_{ji}^*\tilde{u}_i + \mathrm{i}\sqrt{1/2\hbar\omega_j}\mathcal{M}_{ji}\tilde{p}_i \right) \tag{15}$$

which satisfy $[A_j, A_{j'}] = [A_j^\dagger, A_{j'}^\dagger] = 0$ and $[A_j, A_{j'}^\dagger] = \delta_{jj'}$. The eigenvectors of $\tilde{\mathbf{K}}$, and hence the matrix $\boldsymbol{\mathcal{M}}$, may always be chosen to be pure real, but for the moment we have allowed $\boldsymbol{\mathcal{M}}$ to be a complex unitary matrix, for generality. Equations (14) and (15) may be inverted to give

$$\tilde{u}_i = \sum_j \sqrt{\hbar/2\omega_j}\left(\mathcal{M}_{ji}A_j + \mathcal{M}_{ji}^* A_j^\dagger\right) \tag{16}$$

$$\tilde{p}_i = \sum_j \mathrm{i}\sqrt{\hbar\omega_j/2}\left(-\mathcal{M}_{ji}A_j + \mathcal{M}_{ji}^* A_j^\dagger\right). \tag{17}$$

The unperturbed phonon Hamiltonian may now be written in diagonal form as

$$H_z = \sum_j \left(A_j A_j^\dagger + A_j^\dagger A_j\right)\hbar\omega_j/2. \tag{18}$$

We now give every mode j a degree of thermal excitation, defined by the quantity

$$N_j = \langle A_j^\dagger A_j \rangle \tag{19}$$

where the angular brackets designate thermal averaging. The electron–phonon interaction in equations (5) and (10) is then switched on. First-order perturbation theory then leads to two kinds of process. In one, electrons absorb phonons, and in the other, electrons generate phonons. Consider processes in which a single quantum is absorbed out of phonon mode j. The total rate of such processes, within first-order perturbation theory, is [21]

$$\begin{aligned} J_j^- &= (4\pi/\hbar)N_j \sum_{\alpha,\beta=1,2} f_\alpha(1-f_\beta)|\langle\psi_\beta|\Lambda_j|\psi_\alpha\rangle|^2\delta(E_\beta - E_\alpha - \hbar\omega_j) \\ &= (4\pi/\hbar)N_j \sum_{\alpha,\beta=1,2}\int \mathrm{d}E\, f_\alpha(E)[1-f_\beta(E+\hbar\omega_j)] \\ &\quad \times \mathrm{Tr}[D_\alpha(E)\Lambda_j^\dagger D_\beta(E+\hbar\omega_j)\Lambda_j] \end{aligned} \tag{20}$$

where a factor of 2 for electron spin degeneracy has been included and

$$\Lambda_j = \sum_i \sqrt{\hbar/2M_i\omega_j}\mathcal{M}_{ji}V_i, \qquad \Lambda_j^\dagger = \sum_i \sqrt{\hbar/2M_i\omega_j}\mathcal{M}_{ji}^* V_i. \tag{21}$$

Here, we have used the notation $i \equiv n\nu$, introduced earlier, so that V_i is the same as $V_{n\nu}$ in equation (5). Similarly, the total rate of processes in which a quantum is created in phonon mode j is [21]

$$\begin{aligned} J_j^+ &= (4\pi/\hbar)(N_j+1) \sum_{\alpha,\beta=1,2} f_\alpha(1-f_\beta)|\langle\psi_\beta|\Lambda_j^\dagger|\psi_\alpha\rangle|^2\delta(E_\beta - E_\alpha + \hbar\omega_j) \\ &= (4\pi/\hbar)(N_j+1) \sum_{\alpha,\beta=1,2}\int \mathrm{d}E\, f_\alpha(E)[1-f_\beta(E-\hbar\omega_j)] \\ &\quad \times \mathrm{Tr}[D_\alpha(E)\Lambda_j D_\beta(E-\hbar\omega_j)\Lambda_j^\dagger]. \end{aligned} \tag{22}$$

The '1' in the term $(N_j + 1)$ above corresponds to spontaneous phonon emission and is particularly important in the low-temperature limit, $N_j \to 0$. We will return to this point, and

its significance for inelastic current–voltage spectroscopy, later in the paper. The fermionic occupation numbers f_α and f_β take care of the Pauli exclusion principle and arise naturally if second quantization is used [18].

The power into phonon mode j is then given by

$$\begin{aligned} w_j &= \hbar\omega_j J_j^+ - \hbar\omega_j J_j^- \\ &= 2\pi\hbar(N_j+1)\sum_{\alpha,\beta=1,2}\sum_{i,i'}\frac{\mathcal{M}_{ji}\mathcal{M}^*_{ji'}}{\sqrt{M_i M_{i'}}}\int \mathrm{d}E\, f_\alpha(E)[1-f_\beta(E-\hbar\omega_j)] \\ &\quad\times \mathrm{Tr}[D_\alpha(E)V_i D_\beta(E-\hbar\omega_j)V_{i'}] \\ &\quad - 2\pi\hbar N_j\sum_{\alpha,\beta=1,2}\sum_{i,i'}\frac{\mathcal{M}^*_{ji}\mathcal{M}_{ji'}}{\sqrt{M_i M_{i'}}}\int \mathrm{d}E\, f_\alpha(E)[1-f_\beta(E+\hbar\omega_j)] \\ &\quad\times \mathrm{Tr}[D_\alpha(E)V_i D_\beta(E+\hbar\omega_j)V_{i'}]. \end{aligned} \tag{23}$$

Electron coupling to full phonon modes was used in [20], in a density-functional framework, to study local heating in molecular junctions.

As mentioned above, we can choose $\boldsymbol{\mathcal{M}}$ to be real, so that $\mathcal{M}^*_{ji} = \mathcal{M}_{ji}$. We may then obtain the following useful approximate expression for w_j. First, let us ignore any variation in the electron Green functions over energies of the order of $\hbar\omega_j$, enabling us to neglect $\hbar\omega_j$ in the energy arguments of D_α and D_β above. Second, let us assume that we are in the linear voltage regime, where the electron Green functions do not vary significantly over the energy window for conduction, between μ_2 and $\mu_1 = \mu_2 + eW$. Finally, let $|eW| > \hbar\omega_j$. Then, equation (23) reduces to

$$w_j \approx -2\pi\hbar E_j(T^j_{11} + 2T^j_{12} + T^j_{22}) + 2\pi\hbar(|eW| - \hbar\omega_j)T^j_{12} \tag{24}$$

where $E_j = N_j\hbar\omega_j$ and

$$T^j_{\alpha\beta} = \sum_{i,i'}\frac{\mathcal{M}_{ji}\mathcal{M}_{ji'}}{\sqrt{M_i M_{i'}}}\mathrm{Tr}[D_\alpha V_i D_\beta V_{i'}] \tag{25}$$

with D_α and D_β evaluated at the Fermi energy, at zero bias.

2.3. Power into Einstein oscillators

We will now consider electron–phonon scattering and power dissipation, treating the atomic vibrations in a physically very different way. We now imagine that each degree of freedom, ν, of each atom, n, is a separate, independent Einstein oscillator, with an environment-dependent angular frequency, $\omega_{n\nu}$, given by

$$\omega^2_{n\nu} = K_{n\nu n\nu}/M_n. \tag{26}$$

To describe power dissipation into these Einstein oscillators, we may now use the results from the previous subsection, with $\mathbf{K}$ replaced by the diagonal matrix $\mathbf{K}^{\mathrm{EO}}$ with matrix elements

$$K^{\mathrm{EO}}_{n\nu m\mu} = \delta_{nm}\delta_{\nu\mu}K_{n\nu n\nu}. \tag{27}$$

The corresponding matrix, $\boldsymbol{\mathcal{M}}^{\mathrm{EO}}$, of eigenvectors of $\mathbf{K}^{\mathrm{EO}}$, is also diagonal. The power into Einstein oscillator $n\nu$ is given by the following analogue of equation (23) [19]:

$$\begin{aligned} w^{\mathrm{EO}}_{n\nu} &= (2\pi\hbar/M_n)(N^{\mathrm{EO}}_{n\nu}+1)\sum_{\alpha,\beta=1,2}\int \mathrm{d}E\, f_\alpha(E)[1-f_\beta(E-\hbar\omega_{n\nu})] \\ &\quad\times \mathrm{Tr}[D_\alpha(E)V_{n\nu}D_\beta(E-\hbar\omega_{n\nu})V_{n\nu}] \\ &\quad - (2\pi\hbar/M_n)N^{\mathrm{EO}}_{n\nu}\sum_{\alpha,\beta=1,2}\int \mathrm{d}E\, f_\alpha(E)[1-f_\beta(E+\hbar\omega_{n\nu})] \\ &\quad\times \mathrm{Tr}[D_\alpha(E)V_{n\nu}D_\beta(E+\hbar\omega_{n\nu})V_{n\nu}]. \end{aligned} \tag{28}$$

Here

$$N_{n\nu}^{\mathrm{EO}} = \langle a_{n\nu}^{\dagger} a_{n\nu} \rangle \tag{29}$$

is the average number of excitation quanta in Einstein mode $n\nu$, with $a_{n\nu} = (p_{n\nu} - \mathrm{i}M_n\omega_{n\nu}u_{n\nu})/\sqrt{2M_n\hbar\omega_{n\nu}}$. Under the assumptions leading to equation (24), equation (28) simplifies to

$$w_{n\nu}^{\mathrm{EO}} \approx -2\pi\hbar E_{n\nu}(T_{11}^{n\nu} + 2T_{12}^{n\nu} + T_{22}^{n\nu}) + 2\pi\hbar(|eW| - \hbar\omega_{n\nu})T_{12}^{n\nu} \tag{30}$$

where $E_{n\nu} = N_{n\nu}^{\mathrm{EO}}\hbar\omega_{n\nu}$ and

$$T_{\alpha\beta}^{n\nu} = (1/M_n)\,\mathrm{Tr}[D_\alpha V_{n\nu} D_\beta V_{n\nu}]. \tag{31}$$

2.4. The equivalence between the two power formulae

We will now show that, under a broad range of conditions, the full-mode picture of subsection 2.2 and the Einstein picture of subsection 2.3 give the same net power dissipation at any given atom in the system. First, we need to reinterpret the full-mode power formula in equation (23) as follows.

Using (23), the total power, w, dissipated in the junction may be written as

$$w = \sum_j w_j = \sum_i w_i^{\mathrm{proj}} \tag{32}$$

where

$$\begin{aligned} w_i^{\mathrm{proj}} = {} & 2\pi\hbar \sum_{j,i'}(N_j + 1) \sum_{\alpha,\beta=1,2} \frac{\mathcal{M}_{ji}\mathcal{M}_{ji'}^*}{\sqrt{M_i M_{i'}}} \int \mathrm{d}E\, f_\alpha(E)[1 - f_\beta(E - \hbar\omega_j)] \\ & \times \mathrm{Tr}[D_\alpha(E) V_i D_\beta(E - \hbar\omega_j) V_{i'}] \\ & - 2\pi\hbar \sum_{j,i'} N_j \sum_{\alpha,\beta=1,2} \frac{\mathcal{M}_{ji}^*\mathcal{M}_{ji'}}{\sqrt{M_i M_{i'}}} \int \mathrm{d}E\, f_\alpha(E)[1 - f_\beta(E + \hbar\omega_j)] \\ & \times \mathrm{Tr}[D_\alpha(E) V_i D_\beta(E + \hbar\omega_j) V_{i'}]. \end{aligned} \tag{33}$$

In the above, index j runs over all full phonon modes of the junction, and indices $i = n\nu$ and $i' = n'\nu'$ each run over all individual atomic degrees of freedom. The quantity w_i^{proj} is a sum of projected contributions, at atomic degree of freedom i, of the power dissipated into each full mode j. It is natural to interpret w_i^{proj} as the effective net power collected by atomic degree of freedom i. This interpretation may be put on a more rigorous footing as follows. Let

$$\hat{w} = (1/\mathrm{i}\hbar)[H_{\mathrm{z}}, H] = (1/\mathrm{i}\hbar)[H_{\mathrm{z}}, V_{\mathrm{ez}}]. \tag{34}$$

Here, H_{z} is the full phonon Hamiltonian in equation (3), and $H = H_{\mathrm{e}} + V_{\mathrm{ez}} + H_{\mathrm{z}}$ is the Hamiltonian for the coupled electron–phonon system, where V_{ez} is given by equation (5) and H_{e} is the (possibly self-consistent) Hamiltonian for the unperturbed electron system. The quantity $\hat{w}$ is the operator that represents the total power dissipated in the junction. Using the phonon position–momentum commutation relations we may now write $\hat{w}$ as

$$\hat{w} = \sum_i \hat{w}_i, \qquad \hat{w}_i = (1/\mathrm{i}\hbar)[p_i^2/2M_i, V_{\mathrm{ez}}] = -V_i p_i/M_i \tag{35}$$

where, once again, $i \equiv n\nu$ labels a particular atomic degree of freedom. We interpret the quantity $\hat{w}_i$ as an operator that represents the power dissipated by the current-carrying electrons into atomic degree of freedom i. If now we evaluate the expectation of $\hat{w}_i$, within first-order time-dependent perturbation theory, we arrive at equation (33).

We will now show that, under certain conditions, w_i^{proj}, with $i = n\nu$ in equation (33), is essentially the same as $w_{n\nu}$ in equation (28). We choose $\mathcal{M}_{ji}$ in equation (33) to be real, $\mathcal{M}_{ji} = \mathcal{M}_{ji}^*$, as we did earlier, in deriving equation (24). We now make the following approximations. First, we assume that the electron Green functions, and the operators D_1 and D_2, do not vary appreciably over energies of the order of $\hbar\omega$, where ω is a typical phonon frequency. We made the same approximation earlier, in deriving equations (24) and (30). This approximation would be well obeyed, for example, in simple metallic nanocontacts and atomic wires, where $\hbar\omega$ is typically of the order of tens of milli-electronvolts, whereas electron densities of states vary typically on the scale of an electronvolt. An example of a situation where this approximation may break down, on the other hand, is resonant transmission through very narrow quasibound states. If we do make the above approximation, then we may ignore $\hbar\omega_j$ in the energy arguments of D_α and D_β in equation (33). Then the N_j-dependent contributions from the energy integrals in the two terms in that equation largely cancel out. That cancellation may be made complete by our next approximation. Referring back to figure 1, in the steady state, power in equals power out. If we assume that heat is carried out of the junction by normal harmonic lattice heat conduction into the adjoining electrodes, then the characteristic steady-state lattice temperature in the junction may be expected to remain sufficiently low to keep $E_j \ll |eW|$ in equation (24) and $E_{n\nu} \ll |eW|$ in equation (30) [18, 20]. For example, for simple metallic atomic-scale contacts, theoretical estimates predict a steady-state local temperature of the order of 100 K at voltages of the order of a volt (at zero ambient temperature) [18, 20]. Under such conditions, we may ignore the first term in equation (24) and the first term in equation (30). Provided that $|eW| \gg \hbar\omega$, we may, furthermore, replace $(|eW| - \hbar\omega_j)$ by $|eW|$ in equation (24), and $(|eW| - \hbar\omega_{n\nu})$ by $|eW|$ in equation (30). These approximations are equivalent to neglecting $\hbar\omega_j$ in the energy arguments of the electron occupation functions f_α and f_β in equation (33). If we do that, then the N_j-dependent terms in that equation cancel out completely. Assuming for definiteness $\mu_1 - \mu_2 = eW > 0$, this leaves

$$w_i^{\mathrm{proj}} \approx 2\pi\hbar \sum_{j,i'} \frac{\mathcal{M}_{ji}\mathcal{M}_{ji'}}{\sqrt{M_i M_{i'}}} \int_{\mu_2}^{\mu 1} \mathrm{d}E \ \mathrm{Tr}[D_1(E)V_i D_2(E)V_{i'}]. \tag{36}$$

But $\boldsymbol{\mathcal{M}}$ is unitary and, if it is real, it is orthogonal. Hence

$$\sum_j \mathcal{M}_{ji}\mathcal{M}_{ji'} = \delta_{ii'} \tag{37}$$

and therefore

$$w_{i=n\nu}^{\mathrm{proj}} \approx (2\pi\hbar/M_n) \int_{\mu_2}^{\mu 1} \mathrm{d}E \ \mathrm{Tr}[D_1(E)V_{n\nu}D_2(E)V_{n\nu}]. \tag{38}$$

We may now apply the same approximations as those leading to equation (36) above to equation (28) for the power per degree of freedom $n\nu$ in the Einstein picture. If we do that, then equation (28) reduces to precisely the same expression as in equation (38) above, and thus

$$w_{n\nu}^{\mathrm{EO}} \approx w_{i=n\nu}^{\mathrm{proj}} \approx \text{ result in equation (28).} \tag{39}$$

In the linear voltage regime, they both reduce further to

$$w_{n\nu}^{\mathrm{EO}} \approx w_{i=n\nu}^{\mathrm{proj}} \approx 2\pi\hbar|eW|T_{12}^{n\nu} \tag{40}$$

which is equation (30) with $E_{n\nu}$ and $\hbar\omega_{n\nu}$ neglected, in accordance with the assumptions above.

3. Results

In this section, we will test the equivalence of the two power formulae for a specific model system. We will then consider the differences between the full-mode picture and the Einstein-

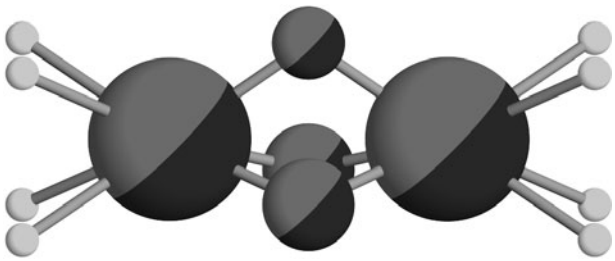

Figure 2. A model conducting structure between two simple-cubic 2 × 2-atom leads (only the surface layer of each lead is shown). The upper semicircle represents the power into the respective atom calculated from equation (33). The lower semicircle represents the power into the atom calculated from equation (28). The power is proportional to the radius of the circle. The largest circle on the plot corresponds to a power of 0.0145 eV ps^{-1}. The voltage is $eW = \mu_1 - \mu_2 = 0.4$ eV. The Fermi level at zero voltage is at $E_F = (\mu_1 + \mu_2)/2 = -2.4$ eV, with the centre of the band chosen as the zero of energy.

oscillator picture away from the range of validity of equation (39). As an illustration, we will calculate the inelastic current–voltage characteristics of model one-dimensional atomic wires.

3.1. A comparison of the two power formulae

The purpose of the numerical calculations below is purely illustrative. We have therefore selected the simplest possible electronic model that allows an electron to be coupled to atomic motion, namely a nearest-neighbour tight-binding model with a single positional basis state, $|n\rangle$, at each atom, n, in the system. The electron Hamiltonian then is

$$H_e = \sum_{m,n} |m\rangle H_{mn} \langle n|. \tag{41}$$

In the present calculations, the hopping integrals, $H_{mn} = H_{nm}$ for $n, m =$ nearest neighbours, are all the same, and equal to $\gamma < 0$. γ is a parameter of the model and is here set to $|\gamma| = 1$ eV. The operator $V_{n\nu}$ in equation (5) takes the form [19, 21]

$$V_{n\nu} = \sum_{m \neq n} (|n\rangle\langle m| + |m\rangle\langle n|) \partial H_{nm} / \partial R_{n\nu}. \tag{42}$$

Here $\mathbf{R_n} = (R_{nx}, R_{ny}, R_{nz})$ is the position of atom n, and the derivatives in equation (42) are evaluated at the equilibrium positions of the atoms. Thus, $\partial H_{nm}/\partial R_{n\nu}$ is non-zero only if m is a nearest neighbour of n, in which case

$$\partial H_{nm}/\partial R_{n\nu} = (\hat{\mathbf{R}}_{\mathbf{nm}})_\nu \gamma' \tag{43}$$

where γ' is the derivative of the nearest-neighbour hopping integral with respect to interatomic distance, and is a parameter of the model. Here, we set $|\gamma'| = 1$ eV Å^{-1}. $(\hat{\mathbf{R}}_{\mathbf{nm}})_\nu$ above is component ν of the unit vector $\hat{\mathbf{R}}_{\mathbf{nm}} = (\mathbf{R_n} - \mathbf{R_m})/|\mathbf{R_n} - \mathbf{R_m}|$. No self-consistency is present in the model. The density of states operators D_1 and D_2 are calculated by the Green function method described in [19].

We now consider the system shown in figure 2. To describe phonon modes within the five-atom structure between the two 2 × 2-atom leads, we associate a simple harmonic spring with each bond shown in the figure. Assuming that each spring is relaxed, the matrix elements of the dynamical response matrix are given by

$$K_{n\nu m\mu} = \begin{cases} -(\hat{\mathbf{R}}_{\mathbf{nm}})_\nu k_{nm} (\hat{\mathbf{R}}_{\mathbf{nm}})_\mu & \text{for } n \neq m \\ \sum_{l \neq n} (\hat{\mathbf{R}}_{\mathbf{nl}})_\nu k_{nl} (\hat{\mathbf{R}}_{\mathbf{nl}})_\mu & \text{for } n = m \end{cases} \tag{44}$$

where $k_{nm} = k_{mn}$ is the spring constant between atoms n and m. In the present example, all nearest-neighbour spring constants are set equal to 7 eV Å^{-2}. All atomic masses are taken to be the same, $M_n = M$, with M set equal to the atomic mass of Au. All on-site energies H_{nn} are set equal to zero.

We now test equation (39) by comparing the power into each atom in the junction, computed directly from equation (28) and from equation (33). The results are shown in figure 2. In each case, the contributions from the three degrees of freedom, $\nu = x, y, z$, have been added up for each atom, n, in the junction. To assign values to the phonon occupation numbers $N_{n\nu}^{\mathrm{EO}}$ in equation (28) and N_j in equation (33), we have assumed a nominal junction temperature of 232 K, somewhat higher than the expected steady-state temperature for a simple metallic nanojunction at the given voltage (at zero ambient temperature) [18, 23], but still within the range of validity of the assumptions of subsection 2.4. $N_{n\nu}^{\mathrm{EO}}$ and N_j are then taken as the Bose–Einstein occupation numbers, corresponding to the phonon angular frequencies $\omega_{n\nu}$ and ω_j, respectively. We see that, if anything, equations (28) and (33) for this system agree even more closely than one might have expected from the seemingly long series of approximations leading to equation (39).

3.2. The differences between the two pictures of atomic vibrations

The practical usefulness of equation (39)—within its range of validity—is that it allows rigorous estimates of local power dissipation based on the much simpler Einstein-oscillator picture. Let us now consider the difference between the full-mode picture of vibrations and the Einstein picture, away from the range of validity of equation (39). A key limit, where this difference is significant, is that of low temperatures and low voltages, with $|eW|$ comparable to $\hbar\omega_j$ for individual phonon modes. In that limit, electron–phonon scattering is controlled by the detailed phonon spectrum $\{\omega_j\}$, and the full-mode picture is essential. As an illustration, we consider the example of point-contact spectroscopy, in which the low-temperature, low-bias inelastic current–voltage characteristics of a nanoscale junction are used as a probe into the phonon spectrum of the junction (see [21] and further references therein).

We go back to the full-mode picture of subsection 2.2, and take the limit of very low lattice temperature in the junction. This eliminates the quantity N_j in equations (20) and (22). The only remaining electron–phonon process is that due to the term arising from the '1' in $(N_j + 1)$ in equation (22). This process is, once again, spontaneous emission of phonons, accompanied by the scattering of an incoming electron into a lower energy state. To satisfy simultaneously the Pauli exclusion principle and energy conservation, this means that for electrons to begin to excite a given phonon mode j, they need an excess energy of at least $\hbar\omega_j$. This in turn requires $|eW| > \hbar\omega_j$. If then we turn the corresponding electron–phonon scattering rate into a backscattered current, and compute the resultant decrease in conductance, in the limit of quasiballistic junctions the inelastic differential conductance may be written as [21]

$$\sigma = \sigma_0 - (e^2/\pi\hbar) \sum_j 4\pi^2 \theta(|eW| - \hbar\omega_j) \operatorname{Tr}[D_1 \Lambda_j D_2 \Lambda_j^\dagger] \tag{45}$$

where D_1 and D_2 are evaluated at the Fermi energy, at zero bias, and σ_0 is the *elastic* zero-bias conductance. The step function θ, defined by $\theta(x) = 0$ for $x < 0$, $\theta(x) = 1$ otherwise, reflects the behaviour discussed above: spontaneous excitation of phonon mode j is switched on as $|eW|$ exceeds $\hbar\omega_j$. Thus, a plot of σ versus W constitutes a map of the phonon spectrum.

Montgomery *et al* [21] studied the inelastic current–voltage characteristics of defect-free metallic atomic chains between two electrodes. It was found that the self-consistent bonding of the chain to the contacts results in a pattern of weak and strong bonds near each chain end. This in turn results in the appearance of localized phonon modes near each chain

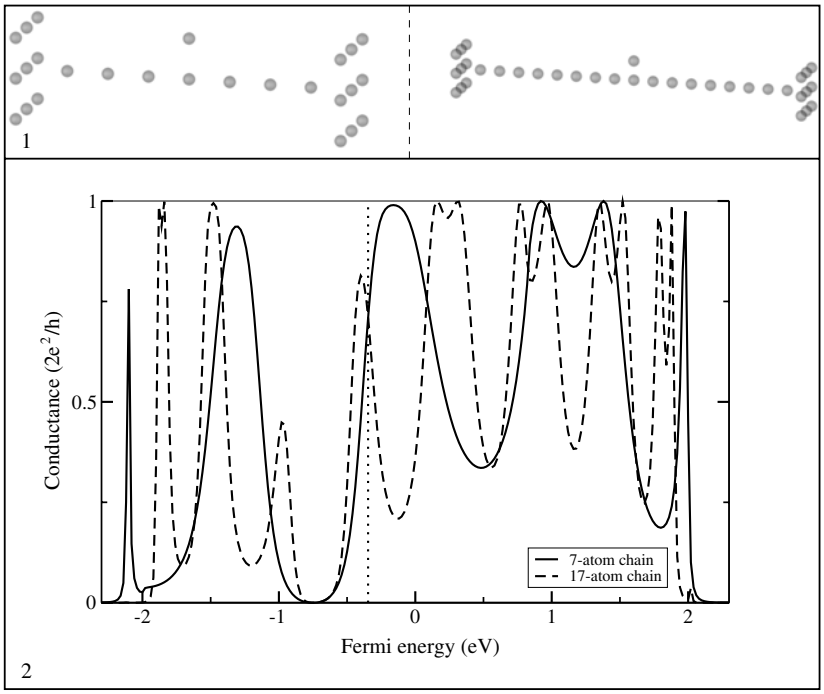

Figure 3. The zero-voltage elastic conductance (panel 2) as a function of Fermi energy of a 7-atom (solid curve) and a 17-atom (dashed curve) chain, with a light atom bonded to the centre atom in each case. The geometries are shown in panel 1.

end, which dominate the inelastic current–voltage spectrum for moderate chain lengths. In a sufficiently long one-dimensional conductor, on the other hand, one may expect electron–phonon interactions to be controlled by extended phonon modes, under the requirement of total momentum conservation [11, 12]. Here, we investigate this crossover in one-dimensional conductors with localized modes of a different origin.

Localized, bound phonons can develop in low-dimensional structures in a variety of situations. For example, an infinite linear chain of identical harmonic springs, with a single spring that is stronger than the rest, may be shown analytically to contain a true bound vibrational mode at the strong bond, with a frequency above the continuous band due to extended phonons. Another example is a linear atomic chain with one atom that has a smaller mass than the rest, in which case a bound phonon mode develops at the light atom. A third example is shown in the top panel of figure 3: a linear chain between two electrodes, with a single light adatom bonded to the chain. As we will see below, there is a localized phonon mode at the adatom, which can give rise to substantial electron–phonon scattering.

The two chains in figure 3 are of length 7 and 17 atoms, attached to 3×3-atom simple-cubic leads. In each case, all atomic masses have been set equal to that of atomic Au, except for the adatom, whose mass is 10% of this value. The simple tight-binding model described above is employed to bond the nearest neighbours of the system. The nearest-neighbour hopping integral and its derivative are once again assigned values of magnitude 1 eV and 1 eV Å^{-1}, respectively. Nearest neighbours within the chain, and between the chain and the electrodes, are considered linked by relaxed harmonic springs of spring constant 7 eV Å^{-2}, as before. All on-site energies are the same and set equal to zero, except that for the adatom which is set to

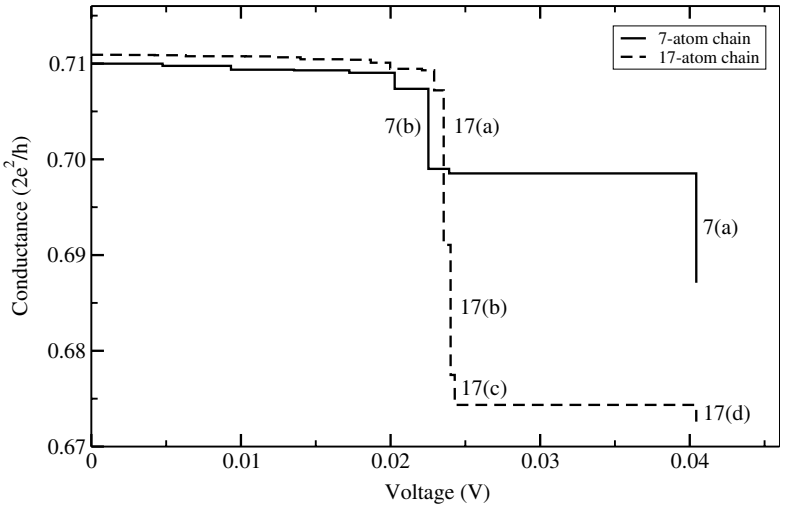

Figure 4. The inelastic differential conductance as a function of voltage for the 7-atom (solid line) and 17-atom (dashed line) geometries shown in panel 1 of figure 3.

-0.75 eV. The band for the perfect linear chain with the present parameters extends from -2 to 2 eV. The zero-voltage elastic conductance plots in figure 3 show that the presence of the adatom results in an antiresonance, at a Fermi energy equal to the on-site energy of the adatom.

The inelastic current–voltage spectra of these systems are now calculated with equation (45). The calculations use a single value for the Fermi energy, indicated by the vertical dotted curve in the conductance plot in figure 3 and chosen to give a similar and relatively high zero-bias conductance for each geometry. Figure 4 shows the inelastic differential conductance as a function of voltage for the two systems. The major features are labelled. A large inelastic conductance drop corresponds to a large electronic coupling to a particular phonon mode. The phonon modes that give rise to the dominant features in figure 4 are shown in figure 5 (for the 7-atom chain) and figure 6 (for the 17-atom chain).

The inelastic conductance of the 7-atom chain shows two dominant features, labelled as 7(a) and 7(b) in figure 4. Figure 5 shows that the phonon mode responsible for feature 7(a) is a localized, trapped vibration, involving the light adatom and its nearest neighbour within the chain. The mode responsible for feature 7(b), by contrast, is an extended mode in the chain. The physics of the coupling of electrons to these two modes is rather different. The chief factor that determines the strength of the coupling of electrons to the trapped mode is the mass of the light adatom. Due to the mass-dependent denominators in equation (21), the lighter the adatom, the larger the value of the term in equation (45) for the trapped mode. The extended mode responsible for feature 7(b), on the other hand, is a conventional extended longitudinal vibration in the chain. The cause of its strong coupling to the electrons may be seen in its wavelength, of about 2 bondlengths. At the present Fermi energy the electron wavelength is about 4.5 bondlengths. Momentum-conserving scattering of electrons of wavevector k and longitudinal phonons of wavevector q requires $2k = q$ [11, 12]. This suggests that feature 7(b) is due to such momentum-conserving scattering. In the present short chain, however, the trapped mode dominates the scattering of electrons.

Imagine now making the chain longer. The coupling of electrons to the trapped phonon mode will remain largely the same, as the physics of that mode does not change. However, as the chain gets longer, both electron and phonon momentum within the chain become better and

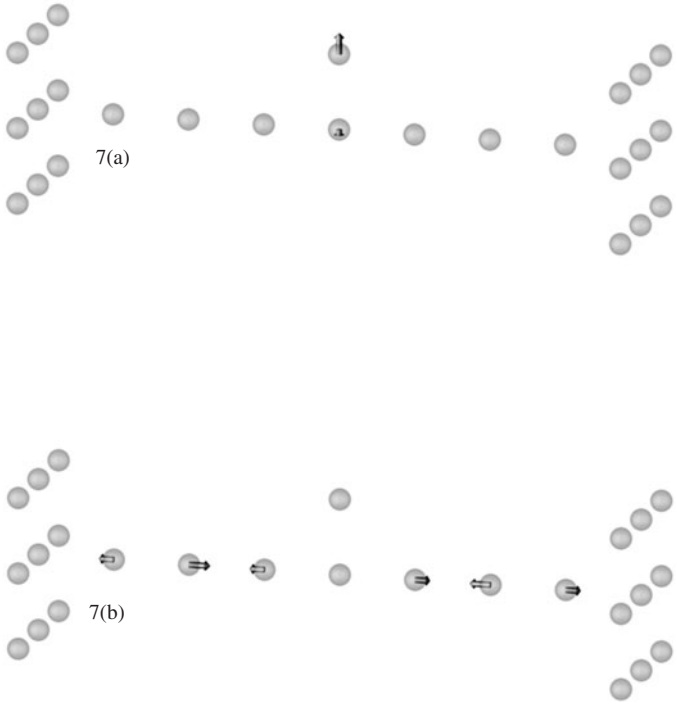

Figure 5. The phonon modes giving rise to the two largest conductance drops for the 7-atom chain, as labelled in figure 4. The arrows, by their length and direction, indicate the relative displacement of each atom in that mode.

better quantum numbers. Therefore, the momentum-conservation selection rule $2k = q$ above, for electron coupling to longitudinal extended modes, will becomes stronger and stronger. This may be seen in the inelastic current–voltage spectrum of the 17-atom chain in figure 4. The plot is dominated by an avalanche of features—17(a), 17(b) and 17(c)—all of which correspond to longitudinal phonons, as seen in figure 6. The modes for the dominant features, 17(a) and 17(b), have wavelengths that closely match the condition $2k = q$. The conductance feature due to the trapped mode involving the light atom, 17(d), now pales into insignificance. Thus, in the long chain, momentum conservation dominates the electron–phonon scattering.

4. Discussion and summary

The goal of this paper is to compare electron–phonon interactions in two extreme pictures of atomic vibrations in nanoscale junctions: full phonon modes versus independent atomic Einstein oscillators. If ω is a typical phonon frequency in the junction and T is the junction temperature, we have shown analytically that in the limit of large voltages, $|eW| \gg \hbar\omega$, and low lattice temperatures, $kT \ll |eW|$, the two pictures produce essentially the same power at a given atom in the nanojunction, subject to the additional requirement that electronic properties do not vary appreciably over energies of the order of $\hbar\omega$. This equivalence turns the computationally and conceptually much simpler Einstein-oscillator picture into a rigorous framework for the calculation of local power dissipation at individual atoms in a nanojunction. This, in turn, makes it possible to identify individual atoms with a greatly enhanced local power [19]. This knowledge is of key importance in addressing the problem of how current flow limits the stability of atomic-scale conductors.

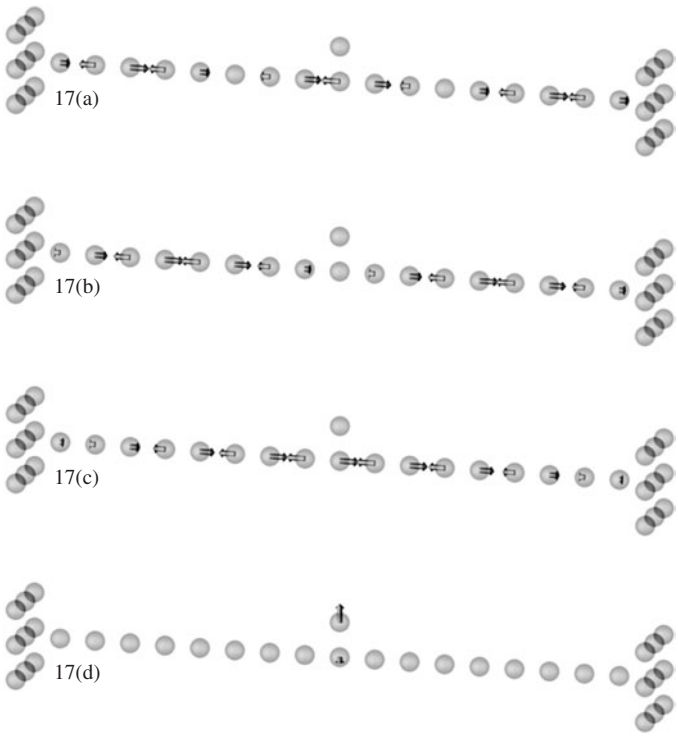

Figure 6. The phonon modes responsible for the largest conductance drops for the 17-atom chain. The labelling of modes is from figure 4.

The full-phonon picture becomes necessary in the limit of low lattice temperatures and low voltages, where electron–phonon scattering is dominated by the detailed structure of the phonon spectrum, as illustrated by the calculations of inelastic current–voltage characteristics presented above. Another situation, in which the equivalence of the two pictures is lost, is the limit of high lattice temperatures, where kT is comparable to eW. Then the first term in equation (24) and in equation (30) may no longer be negligible compared with the second term; it is no longer possible to neglect $\hbar\omega_j$ in the energy arguments of the electron occupation functions f_α and f_β in equation (33), and the algebra leading to equation (39) breaks down. That may occur, for example, in the atomic chains with the light adatom in figure 3. We saw that the adatom gives rise to a trapped localized vibrational mode that couples well to the electrons. Within the harmonic limit, this mode cannot couple to modes in the adjoining electrodes. Hence, there is no mechanism for heat dissipated by the electrons into the trapped mode to be conducted out. In the steady state, equation (24) then sets the thermal energy of that mode to

$$E_j \approx (|eW| - \hbar\omega_j)T_{12}^j/(T_{11}^j + 2T_{12}^j + T_{22}^j), \qquad j = \text{trapped}. \tag{46}$$

In the present case, as a result of the special symmetries of the system, in the limit $|eW| \gg \hbar\omega_j$, this gives $E_j \approx |eW|/4$. Thus, at $W = 0.4$ V, in the harmonic approximation, our trapped mode would be excited to an effective temperature of the order of 1000 K. We have seen that such trapped modes can develop easily in low-dimensional structures. In addition to their role in shaping current–voltage spectra, discussed earlier, localized vibrational modes are likely to act as centres for particularly high local heating and thereby play a particularly important role in limiting the stability of such structures under current flow.

In reality, anharmonicity and electron-mediated phonon–phonon processes would somewhat reduce the temperature of trapped modes below the above estimate, which is to be treated as an upper bound. The analysis of such processes extends beyond the scope of this paper, but, in conclusion, we will pursue the question just one step further. In the lowest-order perturbation theory, considered in this paper, electrons can only ever do one of two things—create a phonon in a given mode, or annihilate one—as reflected by equations (20) and (22). What they cannot do is take an existing phonon and scatter it into a shower of other phonons. Such processes may be studied rigorously by higher-order perturbation theory. However, the Einstein picture above, although it is still a first-order picture, may provide a step in that direction, in the following sense. The lowest-order treatment may be expected to remain valid up to voltages at which the typical lifetime of a phonon due to phonon–electron scattering becomes comparable to a thermal period. In the limit of large W, the phonon lifetime, τ_j, against absorption by the electrons may be estimated from equation (20) as

$$1/\tau_j = (4\pi/\hbar)|eW|\,\mathrm{Tr}[D_1\Lambda_j^\dagger D_2\Lambda_j]. \tag{47}$$

For an Einstein oscillator with a mass of 100 amu and with $\hbar\omega = 0.02$ eV, in a metallic chain under a bias of the order of a volt, τ is of the order of 0.5 ps. At such voltages, extended phonons stop being good quantum numbers: extended vibrations simply do not have time to develop, in between scattering events involving the electrons. Under these conditions, the Einstein picture may be, physically, the better picture. However, as stated above, the high-voltage limit calls for higher-order perturbation theory, or for altogether non-perturbative methods.

Acknowledgment

We are grateful to DEL for support.

References

[1] Agrait N, Yeyati A L and van Ruitenbeek J M 2003 *Phys. Rep.* **377** 81–279
[2] Muller C J, van Ruitenbeek J M and de Jongh L J 1992 *Phys. Rev. Lett.* **69** 140
[3] van den Brom H E, Yanson A I and van Ruitenbeek J M 1998 *Physica* B **252** 69
[4] Yasuda H and Sakai A 1997 *Phys. Rev.* B **56** 1069
[5] Yanson A I, Rubio Bollinger G, van den Brom H E, Agrait N and van Ruitenbeek J M 1998 *Nature* **395** 783
[6] Itakura K, Yuki K, Kurokawa S, Yasuda H and Sakai A 1999 *Phys. Rev.* B **60** 11163
[7] Hansen K 2000 *PhD Thesis* University of Aarhus
[8] Smit R H M 2003 *PhD Thesis* University of Leiden
[9] Nielsen S K, Noat Y, Brandbyge M, Smit R H M, Hansen K, Chen L Y, Yanson A I, Besenbacher F and van Ruitenbeek J M 2003 *Phys. Rev.* B **67** 245411
[10] Heemskerk J W T, Noat Y, Bakker D J, van Ruitenbeek J M, Thijsse B J and Klaver P 2003 *Phys. Rev.* B **67** 115416
[11] Agraït N, Untiedt C, Rubio-Bollinger G and Vieira S 2002 *Chem. Phys.* **281** 231
[12] Agraït N, Untiedt C, Rubio-Bollinger G and Vieira S 2002 *Phys. Rev. Lett.* **88** 216803
[13] Smit R H M, Noat Y, Untiedt C, Lang N D, van Hemert M C and van Ruitenbeek J M 2002 *Nature* **419** 906
[14] Zhitenev N B, Meng H and Bao Z 2002 *Phys. Rev. Lett.* **88** 226801
[15] Ralls K S, Ralph D C and Buhrman R A 1989 *Phys. Rev.* B **40** 11561
[16] Holweg P A M, Caro J, Verbruggen A H and Radelaar S 1992 *Phys. Rev.* B **45** 9311
[17] Chen Z and Sorbello R S 1993 *Phys. Rev.* B **47** 13527
[18] Todorov T N 1998 *Phil. Mag.* B **77** 965
[19] Montgomery M J, Todorov T N and Sutton A P 2002 *J. Phys.: Condens. Matter* **14** 5377
[20] Chen Y-C, Zwolak M and Di Ventra M 2003 *Nano. Lett.* at press
[21] Montgomery M J, Hoekstra J, Todorov T N and Sutton A P 2003 *J. Phys.: Condens. Matter* **15** 731
[22] Todorov T N 2002 *J. Phys.: Condens. Matter* **14** 3049
[23] Todorov T N, Hoekstra J and Sutton A P 2001 *Phys. Rev. Lett.* **86** 3606
[24] Di Ventra M, Pantelides S T and Lang N D 2002 *Phys. Rev. Lett.* **88** 046801
[25] Brandbyge M, Stokbro K, Taylor J, Mozos J L and Ordejon P 2003 *Phys. Rev.* B **67** 193104